

"This is the peer reviewed version of the following article: [Advanced Materials Technologies, 2021, 2020, (10), pp. 1-12] which has been published in final form at [https://onlinelibrary.wiley.com/doi/10.1002/admt.202000665] purposes in accordance with [Wiley Terms and Conditions for Self-Archiving](#)."

Incorporation of Natural Lithium-ion Trappers into Graphene Oxide Nanosheets

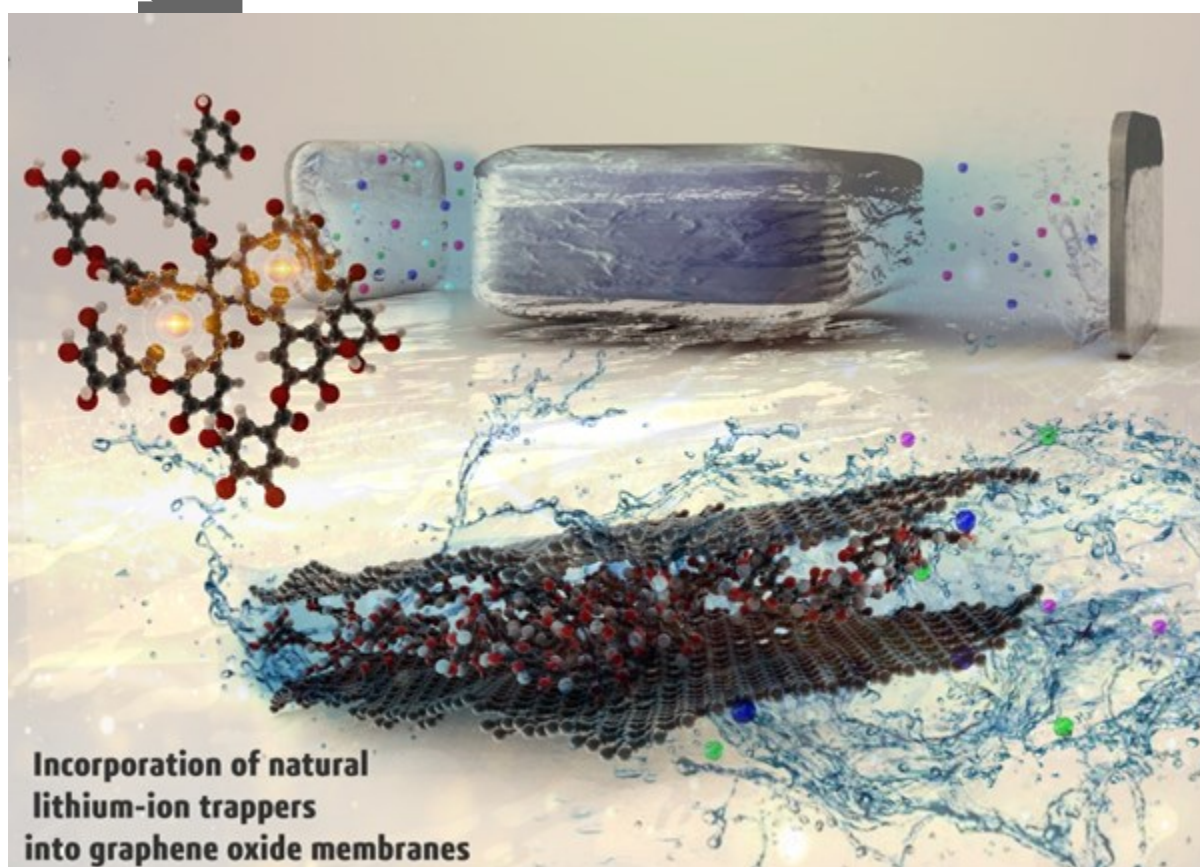
*Hadi Ahmadi¹, Ehsan Hosseini², Withita Cha-Umpong³, Mojtaba Abdollahzadeh¹, Asghar Habibnejad Korayem², Amir Razmjou^{*3}, Vicki Chen^{3,4}, Mohsen Asadnia^{*1}*

H. Ahmadi, M. Abdollahzadeh, Dr. M. Asadnia
School of Engineering, Macquarie University, Sydney, NSW 2109, Australia
Email: mohsen.asadnia@mq.edu.au

E. Hosseini, Dr. A. Habibnejad Korayem
School of Civil Engineering, Iran University of Science and Technology, Tehran, Iran

W. Cha-Umpong, Dr. A. Razmjou, Prof V. Chen
UNESCO Centre for Membrane Science and Technology, School of Chemical Engineering,
University of New South Wales, Sydney, NSW 2052, Australia
Email: amirr@unsw.edu.au

Prof V. Chen
School of Chemical Engineering, University of Queensland, Brisbane, Queensland 4072 Australia



This is the author manuscript accepted for publication and has undergone full peer review but has not been through the copyediting, typesetting, pagination and proofreading process, which may lead to differences between this version and the [Version of Record](#). Please cite this article as [doi: 10.1002/admt.202000665](https://doi.org/10.1002/admt.202000665).

This article is protected by copyright. All rights reserved.

Abstract

Lithium consumption is estimated to face a considerable rise in the next decade; thus, finding new reproducible lithium resources such as brine deposits and seawater has become a fast-growing research topic. However, Li^+ extraction from these resources is challenging due to its low concentration and presence of other monovalent cations exhibiting identical chemical properties. Here, we discovered that tannic acid (TA) inside graphene oxide (GO) nanochannel acts as natural ion trapper, which possesses lithiophilic elements. The lithium-rich feed is achieved by using the potential-driven TA-GO membrane by excluding lithium ions from other monovalent cations. Our results showed that the ion trapping capability of inexpensive TA-GO membrane is $\text{Li}^+ > \text{Na}^+ > \text{K}^+$ with Li trapping energy of -593 KJ mol^{-1} , respectively, where its trapping efficiency goes into a top rank among their expensive synthetic counterparts. Evaluating the combined effect of three key parameters, including barrier energy, hydration energy, and binding energy illustrates that required energy to transport Li-ion through the membrane is higher than that for other monovalent. This proof-of-concept work opens up an avenue of research for designing a new class of ion-selective membranes, based on the incorporation of naturally low cost available lithiophilic guest molecules into 2D membranes.

Keywords: Graphene oxide membrane, Tannic acid, 2D nanochannels, Natural nano net, Lithium separation.

1. Introduction

Increasing demands for the development of renewable energy has attracted many interests to lithium-ion batteries^[1] as one of the most popular rechargeable power suppliers.

Hence, lithium consumption is estimated to increase dramatically in the next decade; therefore, natural lithium resources should be managed in a sustainable way.^[2] Despite the wide range of resources of lithium around the world (e.g. brine deposits, lithium ores and seawater), finding the efficient method to separate lithium from a solution containing chemically similar monovalent ions such as K^+ and Na^+ ions remains challenging.^[3] In contrast, many approaches exist to separate monovalent from divalent, including nanofiltration (NF).^[4]

There are two main approaches for lithium separation, including conventional and membrane technologies. Conventional methods including enrichment, purification and Li^+ precipitation have been used for effective lithium extraction from aqueous resources.^[2, 5] However, they suffer from disadvantages including the poor performance in monovalent selectivity, as well as low lithium concentration in the mentioned natural resources.^[2] On the other hand, nanostructured-membrane technology including several filtration techniques (e.g. reverse osmosis (RO), microfiltration (MF), ultrafiltration (UF), and nanofiltration (NF)) has shown a significant performance for desalination and attracted the attention of researchers in recent years.^[6] Hence, a new approach to this technology is selected as the focus of the present study.

Previously reported studies^[3a] attempted to understand essential design parameters of Li^+ ion-selective membranes including nanochannel dimensions,^[7] morphology,^[8] surface charge,^[9] chemical composition,^[3a] electric double layer, pH, driving force,^[10] ionic strength etc., which should be carefully adjusted during the preparation process. The core design principle of Li^+ -ion selective membranes is based on the reduction of nanochannel size to below Li hydration diameter (0.76nm), which forces the ions to strip their hydration shell partially. It is reported that partially dehydrated Li -ions have more ion mobility than K^+ and Na^+ in nanoconfined areas, and as a result, the membrane could exhibit Li -ion selectivity.^[3a]

Another approach which leads to direct lithium separation is tailoring nanochannels and Li^+ ionophores. The general structure of biological ionophore consists of hydrophilic pores that bind to specific ions to allow them to pass through, while there is no contact between ion and the hydrophobic portion, which interacts with the interior of the membrane^[11]. These macrocyclic compounds binding specific ions in a reversible process are categorised to the natural and synthetic types; where crown ethers as a family of synthetic ionophores found to have similar functions compared to the natural product.^[12] Kazemabad et al.^[13] reported that the ions entirely or partially lose their solvation shell when ions trap in crown ethers. In recent years synthesised crown ethers have been used in a large variety of membranes (e.g. liquid membranes,^[14] plasticized polymeric membranes^[15] etc.) and polymers (e.g. ion exchange resins^[16]) to achieve the goal of alkali metal selectivity. However, critical issues such as leaching the organic solvent in the liquid membrane^[17], polymer-chain rigidity and high cost hindered their practical applications for large scale ion separation, and limited their use to sensing systems.

GO membranes are known as an excellent candidate to intercalate with a variety of guest molecules, including ionophores. The intercalation of ionophores into GO membrane stands on two different strategies. The first one is to incorporate K^+ , and Na^+ ionophores mainly crown ether moieties into a membrane matrix that can form complexes with the alkali metals except for lithium resulting in a lithium-rich permeate.^[13] On the other hand, to have a lithium-rich feed, lithium ionophores can be used to hold Li^+ while providing facile transport of K^+ and Na^+ . This concept was studied by Bang et al.^[18] who used the crown ether-intercalated GO membrane. Crown ether molecules (dibenzo-18-crown-6) binding to K^+ ions were employed as synthetic ionophore. This approach showed a satisfactory level of salt rejection (e.g., Na^+) and water permeation. Although the addition of synthetic crown ethers could lead to a high cation-selective membrane, disadvantages such as high cost and poor

long-term stability associated with the ionophores, have hindered the crown ethers-based cation-selective membranes commercial applications. Hence, replacing them with a justifiable alternative contributes to more effective designs.

To understand the transportation mechanism of ion inside the nanochannels, knowing parameters controlling the mass transport is the main priority. Besides internal geometry and surface chemistry of nanochannels,^[3a, 19] other advantageous parameters, such as establishing a multi-component structure inside nanochannels by introducing various guest molecules attract more attention.^[20] Recently, the incorporation of certain additives with GO-based nanosheets has provided several applications for these 2D membranes. For instance, significantly improved nanofiltration properties and desalination capabilities^[21] were reported as a result of employing natural polyphenols such as tannic acid^[22] and polydopamine.^[23] However, the use of some guest compounds is limited by various compelling challenges such as their high cost and non-uniform distribution of particles in a confined area when industrialization is a criterion.^[3a, 19]

In this paper, the inclusion of a natural crown ether-like structured ion trapper (natural ionophore) in GO membrane has led to the strategic design of 2D material followed by the process of achieving the lithium-rich feed. Thus, the primary goal of this paper is to fundamentally study the formation of complexes and ion transportation mechanism, which can trap lithium in Graphene Oxide nanosheets. Herein, we have discovered that inexpensive tannic acid molecule acting as the natural cation nano net has a built-in crown-like element that can serve to trap Li-ion while allowing K^+ and Na^+ to be conducted, resulting in a lithium-rich feed. This finding can emerge as a new class of natural ionophores. Furthermore, the recent studies on the application of tannic acid in the improvement of Li-ion separation show that the Polypropylene (PP) membrane coated with TA as a natural polymer exhibits more hydrophilicity which leads to higher ion conductivity.^[24] Among all the studies

investigating various aspects of GO membrane, the introduction of TA to these membranes as a guest molecule has attracted the researchers' interest. The TA-GO membranes have shown the enhanced capability of separating monovalent ions (e.g. K^+) from divalent ions (Ca^{2+} , Ni^{2+} , Mg^{2+}) as well as dye separation with high efficiency. Furthermore, increased stability in aqueous solutions regardless of pH and elevated water permeation were attributed to TA presence inside GO layers.^[25] Coating a TA polymeric layer on the surface of GO through oxidative polymerisation^[25a, 26] results in stabilization of the mechanical properties of the nanofluidic membrane through the reaction between the hydroxyl groups of TA with epoxy groups in GO. Incorporating tannic acid into GO nanosheets to construct a stable membrane-like morphology is utilized to fabricate the GO membranes designed in this study. The pressure-driven filtration systems used in the previous studies^[18, 25] are not suitable for ion transportation applications due to a number of drawbacks and challenges such as the potential of structure collapse, reduction of nanochannel size due to nanosheets compaction and escaping the incorporated guest structures from nanochannels, which result in a considerable separation efficiency drop.^[19] Therefore, an electric potential-driven system instead of a pressure-driven system is used for the first time in the present study to evaluate the monovalent separation performance of TA-GO membrane for its potential to achieve higher ion separation efficiency.

In addition, in this study, we investigated for the first time the effect of the natural cation nano net formation resulted from the induction of TA inside GO nanolayers on the exclusion of Li^+ from other monovalent cations. Furthermore, for a better insight of Li^+ transportation mechanism, molecular dynamic (MD) simulation was employed to predict tannic acid diffusion barrier against ions to penetrate through the nanochannel. In good agreement with experimental data, this finding reveals that the membrane capability to trap Li-ion is higher than its potential to hold other monovalent. The results of this study introduce

the new concept of the ion trapping mechanism through nanochannels to improve the selection/extraction of Li^+ from other ionic compounds.

2. Results and discussions

After fabricating the TA-GO membrane by dispersing the mixture of 1 mg/ml of tannic acid and 0.02 mg/ml GO in Milli-Q water and filtering through the polypropylene substrate using vacuum filtration process (Figure S1), the resultant membrane was subjected to characterization tests including XRD, FTIR, TGA, SEM and AFM to identify the size, morphology, surface topography, functional groups and crystalline structure.

As one of the most important parameters in conductivity measurement, the interlayer spacing of the nanochannels was evaluated under various conditions to obtain an accurate estimation of the cross-sectional area through which the ionic flow is passing. As demonstrated in **Figure 1a** and **1b**, by soaking the TA-GO membrane in deionized water and 1M KCl solution, the d-spacing of nanochannels does not change from that of a fresh dry membrane (11.48 Å). The results show that the swelling of GO layers can be significantly minimised or even eliminated by functionalizing with tannic acid, as the interlayer spacing does not change after being exposed to Milli-Q water (black and green lines in Figure 1a). However, the nanochannel d-spacing is deducted to 8.93 Å due to a slight reduction of graphene oxide sheets after being re-dried in a hot chamber at 85 °C, which is associated with water and OH groups desorption.^[27] From FT-IR, as shown in Figure 1c, the tannic acid-functionalized GO composite membrane appeared to have a more explicit C-O bond at around 1240 cm^{-1} than that of GO composite membrane (see Figure 1d). The peak also appears at 760 cm^{-1} for the GO membrane with tannic acid, which is the C-H out-of-plane bend of the phenyl group.^{[24,}
^{28]} Other peaks at approximately 3400, 1720, and 1625 cm^{-1} are C-OH hydroxyl stretch, C=O carboxyl stretch, and C=C carbon stretch, respectively. The peaks at 1370, 1240 and 1050

cm-1 are C-O stretch (epoxy and alkoxy groups), respectively.^[28a] In terms of thermal analysis as indicated in Figure 1e, the presence of tannic acid inside the GO layer increased the onset of thermal degradation by approximately 21°C from the GO membrane without tannic acid and 40 °C from the PP membrane without GO coating. This improvement in thermal stability of TA-GO membrane is followed by widening the temperature range of the degradation in TA/GO/PP compared to GO/PP due to the reduction of GO and the interactions between GO and tannic acid molecules.^[29] Also, the temperatures where 50% of the samples had been decomposed were at 234 °C, 277 °C, and 318 °C for PP, GO/PP and the TA/GO/PP membrane, respectively.

As shown in Figure 1f, a flexible rectangular-shaped strip of TA-GO membrane 5mm wide and 15mm long was cut from the thin film and prepared for mounting in the ED cell. The SEM images presented in Figure 1g and 1h, show the cross-sectional and top view of the membrane. Based on this characterisation, it can be confirmed that the GO layers are laterally stacked on each other, and the top surface is free of cracks. As shown in Figure 1i, the height profiles obtained from the atomic force microscopy (AFM) image in two different directions indicate the monolayers of TA-GO nanosheets are almost flat, with uniform thickness around 1.4 nm. The average surface roughness of the tannic acid-functionalized GO composite membrane is measured to be 97.3 nm. The water contact angle for the GO membrane is around 75°. However, for the tannic acid-functionalized GO membrane, the water droplet was absorbed into the GO layer in 2 s after dropping, making the membrane super hydrophilic.^[30]

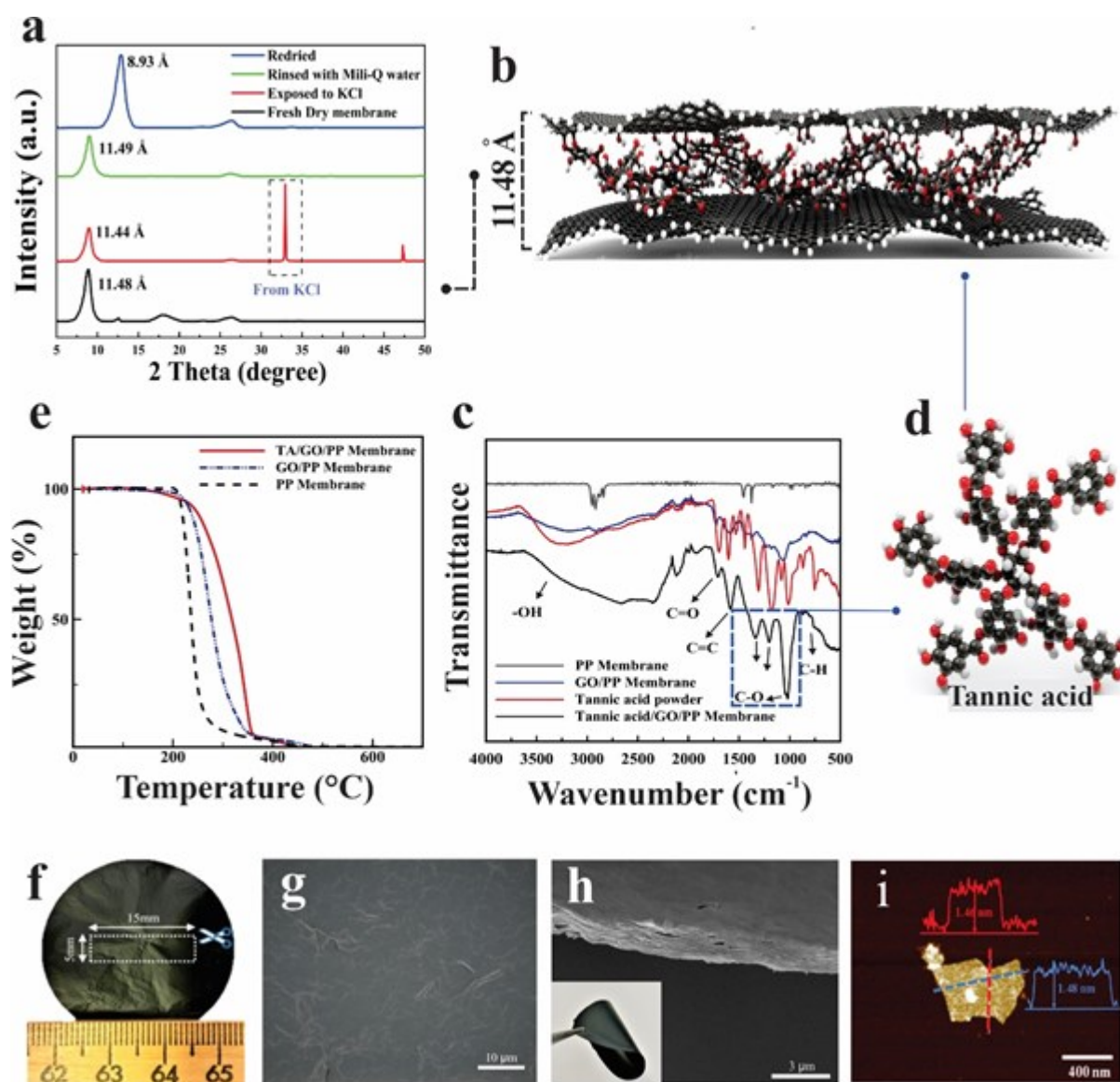


Figure 1. Characterisation of fabricated TA-GO membrane. (a) XRD patterns of a fresh dry TA-GO membrane (black line), hydrated TA-GO membrane exposed to 1M KCl (red line), rinsing the exposed TA-GO membrane with Milli-Q water (green line) and redried TA-GO membrane (blue line), (b) Molecule view of TA inside GO nanochannel size. , (c) FTIR spectra of a TA-GO/PP membrane (black line), a GO/PP membrane (blue line), and PP membrane (grey line), (d) Schematic illustration of TA structure and functional groups. , (e) Thermogravimetric analysis (TGA) of TA-GO/PP membrane (red line), a GO/PP membrane (dashed blue line), and PP membrane (dashed black line), (f) Digital photograph of the rectangular-shaped strip with specific dimensions on TA-GO film, (g) SEM image of TA-GO membrane from the top view, (h) Cross-sectional SEM image of flexible TA-GO membrane, (i) AFM image of a single layer TA-GO sheet and the corresponding height profile in two different directions.

As shown in the snapshot of membrane design and elements presented in **Figure 2a**, after degassing process in a vacuum chamber, the membrane is sandwiched between two layers of PDMS and cured in the oven to prevent the effect of leakage in the test setup. This step was followed by carving the two reservoirs (with a volume of 1.0 mL) at each end of the

membrane to expose it to an electrolyte solution, with the Ag/AgCl electrodes inserted into the reservoirs. The schematic image of the TA-GO membrane and ED cell and an image of the experimental setup are presented in Figure S2. Several LSV tests were conducted to ensure the membrane is not conductive in dry condition (see Figure S3). The linear current-voltage curves (I-V) obtained from centimeter-long TA-GO ED cell at various concentrations of KCl is plotted in Figure 2b. The linear trend of the curves shows that no hydrogen reduction occurs around the electrodes,^[31] and due to effective insulation between the membrane and PDMS, the channels surrounded by the lamellar layers is the only passage for the ionic flow (See Figure 2a). The results at four different concentrations show that the current measured at each specific voltage signal is increases proportionally with the electrolyte concentration. The conductance values resulting from inverting the electrochemical resistance of the membrane, produce the graph of ionic conductivity for salt (KCl) concentrations ranging from 10^{-6} to 1 M, as shown in Figure 2c. It is observed that the bulk solution conductivity is proportional to the electrolyte concentration, which is in agreement with previously published studies.^[32]

In addition, as can be seen in Figure 2c, the membrane conductivity behaves distinctively for high and low concentrations. At concentrations of 0.1 M and higher, the membrane conductivity trend resembles the bulk solution; however, in lower concentrations, the membrane conductivity diverges from bulk and at concentrations about 0.01 M almost plateaus. This accounts for the membrane's surface-charged-governed ion transport characteristic, due to a Debye screening length comparable to the dimension of nano channel's d-spacing. Thus, at low ionic strength, due to high thickness of the electric double layer (EDL) on the nanochannels, as well as their negative charge, the counterions (cations) are selected while the other co-ions (anions) are repelled.^[32b] At high ionic strength, EDL

compresses and its overlapping disappears resulting in opening up the nanochannel, thus resembling bulk behavior.

The conductance of a single nanochannel (G_0) is calculated based on the summation of surface conductance (G_S) and bulk conductance (G_B) divided by the number of nanochannels, where the portion of each term varies due to changes of electrolyte concentration. According to the formula reported in the literature,^[32b, 33] this value can be obtained as below.

$$G_0 = G_B + G_S \quad (1)$$

$$G_B = q(\mu_c + \mu_a)C_B N_A w h_0 / l \quad (2)$$

$$G_S = 2\mu_c \sigma_s (w / l) \quad (3)$$

where μ_c and μ_a are the mobility of cation and anion respectively; C_B is bulk concentration, N_A is Avogadro's number, h_0 is the effective height of single nanochannel, w and l are the width and length of the channel, σ_s is surface charge density and q is an elementary charge. At high concentration, the effect of surface charge is negligible compared with the bulk solution. On the other hand, by decreasing the concentration, the conductance of the surface dominates, and the total conductance is calculated based on those ions passing through the EDL. At low concentrations, cations are absorbed in the nanochannel due to the negative charge of the surface and consequently ionic flow is increased, resulting in the deviation of surface conductance from bulk conductance until the plateau is reached. At transient concentration ($C_t \sim 0.01$) where the surface and bulk conductance are equal, the surface charge density can be determined as

$$\sigma_s = C_t N_A q h_0 \quad (4)$$

where the effective height of single nanochannel (h_0) is calculated by subtracting the thickness of graphene basal plan (approximately about 0.35 nm^[34]) from the channel d-

spacing suggested by XRD results presented in Figure 1a. Although it has been reported that the interlayer spacing can be affected when the membrane is exposed to different salt electrolytes,^[35] here it is shown that for KCl the swelling of nanochannels is negligible and minimum d-spacing remains around 1.144 nm. So the minimum effective thickness of a single nanochannel (h_0) would be around 8 Å which is large enough to pass the monovalent ions such as K^+ , Na^+ and Li^+ with a corresponding hydrated diameter of 6.62 Å, 7.16 Å and 7.64 Å through the nanolayers without removing their hydration shell. Assuming the total effective thickness of nanochannels exposed to KCl equal to 1.07 μm by equalizing the total conductance with bulk conductance, the effective number of nanochannels is obtained as $h_{total}/h_0 = 1347$. Thus, based on Equation 4, the surface charge density (σ_s) is estimated to be 0.76 mC/m². In order to find the cation mobility (e.g. K^+), the surface charged-governed-like behaviour should be assumed for calculation of single layer conductance of TA-GO membrane (see Equation 3) which results in $\mu_c = 1.1 \times 10^{-3} \text{ cm}^2 \text{ V}^{-1} \text{ s}^{-1}$ (see details of calculations in section 3.2 of supporting information).

Due to the reciprocal proportion of EDL thickness with the square root of ionic strength ($\lambda_D = 0.304/\sqrt{I}$ at 25 °C), the membrane bulk conductance is profoundly affected by the valence of salt components (see details in section 3.3 of supporting information). Based on Equation 5, since the value of ionic strength for electrolytes including divalent (CaCl₂ and MgCl₂) is triple those of comprising monovalent (KCl, NaCl and LiCl), the divalent concentration is considered as one-third of monovalent to perform conductivity tests while maintaining a similar ionic strength (I=1 M) for all electrolyte solutions.

$$I = \frac{1}{2} \sum_{i=1}^n c_i z_i^2 \quad (5)$$

where c_i is the molar concentration of ion i and z_i is the charge number of that ion. Thus, to evaluate the performance of the ED cell on the transmissibility of ions of different ionic

properties (e.g. size and charge), five different solutions containing KCl, NaCl, LiCl with 1 M concentration and CaCl₂ and MgCl₂ with 0.33 M concentration at I=1 M were measured separately, with ionic currents and conductance reported in Figure 2d, as I-V curves.

The slope of the curves shows that the TA-GO membrane has the lowest conductivity for Mg²⁺, while Li⁺ shows the minimum value among monovalent ions. The I-V curves obtained through LSV test are confirmed using the outputs of electrochemical impedance spectroscopy test (EIS) as shown in Figure 2e. The EIS technique is based on the impedance measurement of the system and applies an altering current (AC) signal to the counter and working electrodes to measure the impedance of the cell.^[3b] As presented in Figure 2e, it can be observed that the maximum resistance is plotted for Mg²⁺ ions which mean the lowest conductivity of membrane as reported using LSV tests. Figure 2f shows the ion transportation mechanism with and without the introduction of the tannic acid structure inside the GO nanolayers. A closer look illustrates that the ions experience multiple dehydration-hydration when they are passing through the TA structure, which strongly affects the membrane's selectivity.

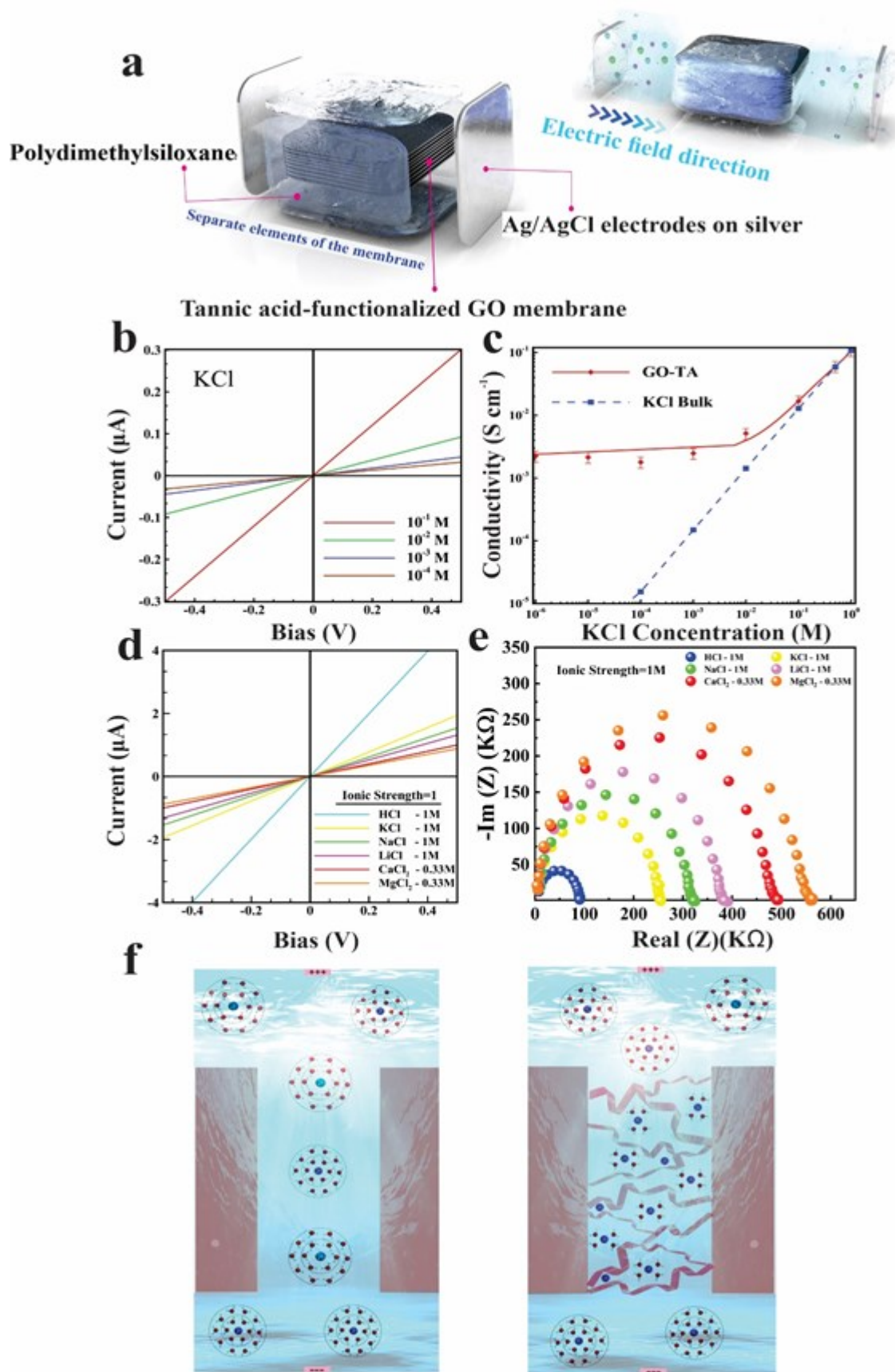


Figure 2. Ion transportation through TA-functionalized GO nanochannel. (a) Schematic view of separate

elements of the membrane and snapshot of membrane design for ionic flow., (b) Representative I-V curves obtained at different KCl concentrations from 10^{-4} to 10^{-1} M, (c) Ionic conductivity as a function of the KCl concentration from 10^{-6} to 1 M, (d) A comparison between I-V curves of TA-GO membrane recorded for different electrolyte solutions at the same ionic strength, (e) Nyquist plots of TA-GO membrane recorded for different electrolyte solutions at the same ionic strength, (f) Ion transportation mechanism through GO nanochannels with/without the presence of TA (spheres: light blue= Cl^- , dark blue = cation ions that are surrounded by H_2O molecules. “+” sign is Cathode while “-” sign is Anode).

The variation of conductance versus hydrated diameter of different cations is investigated in **Figure 3a**. Based on the properties of metal ion reported in the literature^[36] (see Table S1), the highest conductance value is around $3.9 \mu\text{S}$ for K^+ , being the smallest hydrated ion, compared with $1.6 \mu\text{S}$ for Mg^{2+} which has the largest hydrated diameter. Using the conductance values as presented in Figure S4, the selectivity ratio for different ions is formulated below,

$$\text{Ion Selectivity Ratio} = \frac{G_{M_i, \text{Cl}}}{G_{M_j, \text{Cl}}} \quad (6)$$

where G is the conductance, M is a cation, and i and j represent each cation in order Li^+ , Na^+ , K^+ , Ca^{2+} and Mg^{2+} . As indicated in Figure 3b, the selectivity ratio of Li^+/K^+ , Li^+/Na^+ , $\text{Li}^+/\text{Ca}^{2+}$ and $\text{Li}^+/\text{Mg}^{2+}$ is calculated as 0.67, 0.85, 1.31 and 1.49, respectively. The comparison of the selectivity ratio between monovalent ions shows that the permeation of Li^+ ions is less than Na^+ and K^+ ions. This results in lithium enrichment in the feed reservoir, particularly when the feed is free of double-charged ions. Also, the Li^+ ion will be selected from Ca^{2+} and Mg^{2+} when no other monovalent ions are present in the feed. This state of Li^+ ion selectivity leads to Li^+ -rich permeation in the permeate side. These findings can be explained through the investigation of parameters that manipulate the membrane's selectivity. Nanochannel size has been reported as one of the most important parameters affecting Li^+ -ion selectivity. Razmjou et al.^[3a] stated that in the absence of any charge on the inner wall surface of nanochannel, the dimension of the nanochannel must be smaller than the hydrated diameter of Li^+ (around 0.764 nm) in order to induce Li^+ selectivity. It has been reported that

at this point, the movement of alkali metal ions is mainly affected by the ions' partial dehydration, which is consistent with ion selectivity for a non-charged nanochannel.^[37] However, the above condition can be altered when the nanochannel surfaces have a negative charge. In this state, in addition to ion dehydration, other parameters such as ions' affinity to the functional groups should be taken into account to effectively study the ion transport mechanism. However, as presented in Figure 3c, the interlayer spacing of nanochannels in dry conditions and when exposed to different electrolyte salts exceeds the hydrated diameter of Li⁺-ion, with a spacing of 11.44Å, 11.83Å, 12.43Å, 12.44Å and 13.72Å for KCl, NaCl, CaCl₂, MgCl₂ and LiCl, respectively. Given the size of these nanochannels, it is unlikely that the ions experience significant partial dehydration so other contributory factors should be considered.

Surface charge is another major parameter which can influence the behaviour of Li-ions inside the nanochannel. Here, a negatively charged GO-based membrane containing hydroxyl and carboxyl groups in its lamellar structure facilitates the transport of counterions with a positive charge, while ions with a negative charge are impeded. As presented above, the calculation of EDL thickness as a function of ionic strength shows that it is about 0.304 nm on the nanochannel's surface.^[38] Considering the total thickness of EDL in a single nanochannel (~0.608) and width of single GO nanosheet (~ 0.35), it can be concluded that EDLs are close to each other in the nanochannel, yet they do not entirely overlap. Thus, the role of tannic acid introduction as a guest molecule between GO nanolayers can be highlighted as an effective parameter to modify the selectivity of the nanochannel. This phenomenon will be comprehensively justified using MD simulation in the following section.

As mentioned, ion permeation tests were carried out through an ED cell with a horizontal-arrangement TA-GO membrane embedded between two reservoirs filled with Milli-Q water and the mixed salt solution respectively, including similar amounts of KCl,

NaCl, LiCl, MgCl₂ and CaCl₂ at 0.5 M concentration. As shown in Figure 3d, the trend obtained by electrochemical tests is confirmed by the inductively coupled plasma (ICP) test, where the K⁺ and Mg²⁺ ions show maximum and minimum permeation rates, respectively.

Considering the results provided by selectivity and permeation tests, Table S2 shows a comparison of ion selectivity in terms of Li⁺ ion trapping ratio between TA-GO membrane and other nanostructured 2D membranes reported in the literature. It can be seen that the TA-GO membrane presents either better performance in lithium recovery from the enriched feed or less complicated synthesizing process. Moreover, the trapped Li⁺ ions in the nanochannels can be recovered from the system by placing Milli-Q water on the permeate side and reversing the direction of the electric field to discharge the ions. In terms of membrane stability, as shown in Figure S5, the membrane conductance measured for 1M solution of KCl and LiCl is reproduced after an extended period of time, which indicates its adequate performance in the long term.

Author Manuscript

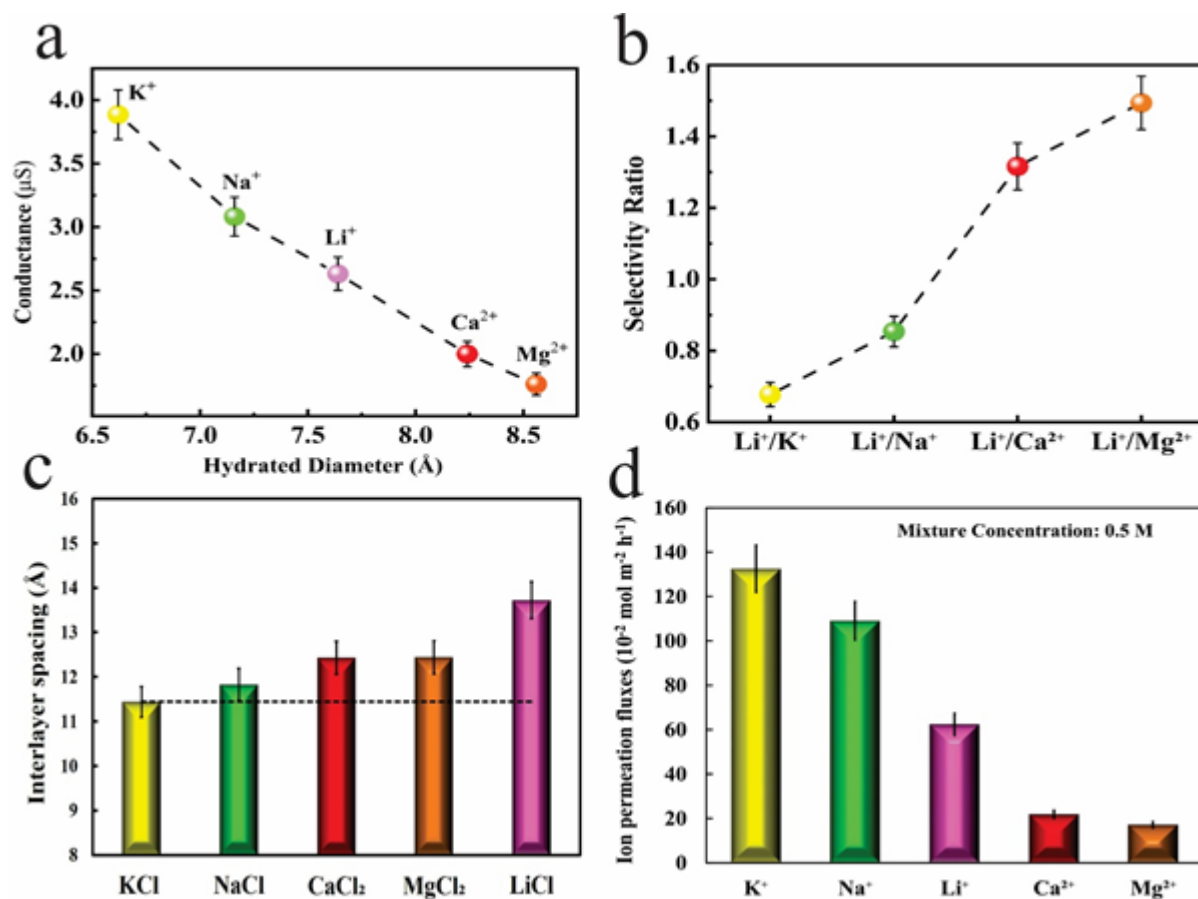


Figure 3. Effect of hydrated radii and chemical properties of cations on the transportation behaviour through the TA-GO nanochannel, (a) Variation of membrane's conductance with hydrated diameter of cations, (b) Comparison between the measured selectivity ratio of Li⁺ to other cations, (c) Variation of nanochannel d-spacing due to exposing the TA-GO membrane to 5 different salt solutions, (d) Evaluation of ion permeation fluxes of 0.5 M mixed salts solution through TA-GO membrane at 1.0 V applied electric field using an ICP test.

3. Molecular dynamics simulation

MD simulation was conducted to evaluate different ion transport characteristics to fundamentally study the ion transportation mechanism of introducing TA into the GO nanochannels. The initial configuration of the simulation system and the distribution of tannic acid as a pattern of the net in the GO membrane were presented in Figure S6 and S7, respectively. Based on the MD findings, a new concept of ion transportation entitled the natural cation nano net was discovered and described for the first time in this study. Nano nets with extremely confined cavities are produced by chain entanglement between graphene

oxide and tannic acid. It is seen that presenting tannic acid inside the graphene oxide nanosheets act as a pattern of the purposeful energy barrier to the diffusion of cations. This process occurs due to the intrinsic structure of tannic acid, which is like continuous crown ethers along the membrane that directly achieve optimal ion transport conditions, i.e., maximum current densities and selectivity.

Figure 4a depicts the arrangement of tannic acid inside graphene oxide, where tannic acid experiences molecular packing and angle change achieving optimized condition under interaction with the graphene oxide. Due to the tannic acid diffusion barrier, permeation of cations inside the TA-GO membrane is difficult and depends on several parameters such as barrier energy, hydration energy and binding energy; where the first two represent the resistance against ions entering the nanochannel, and the last is the energy required to disassemble the ions absorbed into the TA-GO structure. The tannic acid behaviour was traced in the interlayer space of graphene oxide, and it was discovered that tannins and phenol groups as the building blocks of tannic acid in the interlayer confined space of graphene oxide create specific traps such as crown ether. This process, illustrated in Figure 4b and c, can produce the ion trap and diffusion barrier for cations. Figure 4d shows the barrier energy to ions, where the barriers are considerably larger for divalent ions than monovalent ions. The level of barrier energy on penetrating to the narrow capillary membrane for Mg^{2+} , Ca^{2+} , Li^+ , Na^+ and K^+ are 113, 90, 38, 43, and 40 $KJ mol^{-1}$, respectively. The trends exhibited in barrier energy suggest that the extent of the barrier for ions is related to the hydration energy. The larger charges on Mg^{2+} and Ca^{2+} ions result in a stronger electrostatic attraction between the ions and water molecules in the hydration of ions, and the level of these absorptions is reflected in the extent of their hydration energies (see Table S1). So, cation ions with the largest negative hydration energies have the largest barriers for permeation. Hence, as shown in our experiments, the diffusion of monovalent (Li^+ , Na^+ and

K^+) ions in nanochannels occurs more readily than divalent ions (Mg^{2+} and Ca^{2+}), resulting in higher conductivity. In general, ions after incomplete dominance on barriers energy experience substantial dehydration in the membrane. The noticeable trend in this dehydration is that the amount of dehydration over the membrane is very changeable due to the size of cavities. The passable cavities are formed from the stereoregular atoms that have been adopted by chain entanglement between graphene oxide and tannic acid. Figure S8 demonstrates a big trajectory of water molecules in different areas inside of the TA-GO membrane. The water molecules' distribution along the membrane is fragmented and creates nanoscale groups of water. The average hydration energy of ions is illustrated in the TA-GO membrane in Figure 4e, where the hydration energy of ions is approximately halved. The amount of hydration energy for Mg^{2+} , Ca^{2+} , Li^+ , Na^+ and K^+ are -631, -493, -267, -209, and -163 $KJ mol^{-1}$, respectively. These results show that ions experience considerable dehydration, where the binding energy between ions and the TA-GO membrane is very large (see Figure 4f). Comparing the amount of binding energies with hydration energy probably supports our hypothesis that TA-GO enables a nano net for trapping ions. In Figure 4g, the radial distribution function (RDF) shows the distance of oxygen atoms in water molecules around the cations inside the TA-GO membrane while the inset shows the distance of oxygen atoms in TA-GO with cations. The maximum peaks of the RDF for oxygen atoms in water molecules (O_w) surrounding Mg^{2+} , Ca^{2+} , Li^+ , Na^+ and K^+ are at 2.05, 2.33, 1.89, 2.31 and 2.73 Å, respectively. The height of RDF peaks for Mg^{2+} and O in water and also Ca^{2+} and O in water are higher than that of monovalent ions with O in water. This means that more water molecules are in the first hydration shell of Mg^{2+} and Ca^{2+} compared to that of Li^+ , Na^+ , and K^+ , in which leads to the formation of a dense water cluster in the first hydration shell of Mg^{2+} and Ca^{2+} . However, due to the difficult exchange of the water cluster with the encircling water, the distance between the hydrated cations and the oxygen functional group

on the TA-GO is equal to the distance of the first hydration shell. As mentioned in Figure 4g, Mg^{2+} and Ca^{2+} have a stronger interaction with the hydroxyl group and oxygen atoms in tannic acid resulting in higher peaks than the monovalent ions.

To determine the effect of the electric field on the transport of ions, we used three different rates of the electric field. Figure 4h shows the selectivity of K^+ to other ions under the electric field. The K^+ ion in the presence and absence of the electric field shows a significant selectivity ratio, such that the selectivity of the K^+ ion relative to the Mg^{2+} is about 9.1, 5.6 and 3.9 times under the electric field with the rates of 0, 0.5, and 1 V/Å, respectively. Generally, applying an electric field to the process of transfer increases transport efficiency as seen in the experimental results (see Figure 3a and 3b), but the increase in the voltage rate of this external driving force results in a decrease of the selectivity ratio. Moreover, comprising the selectivity ratio of K^+ ion relative to the Li^+ ion under 1 V/Å electric field shows a very good agreement between experiments and MD simulation results. However, it should be noted that the MD results are provided in an ideal condition, and the important role of probable defects and distortion in nanolayers for selectivity measurement of the actual system should not be ignored.^[39]

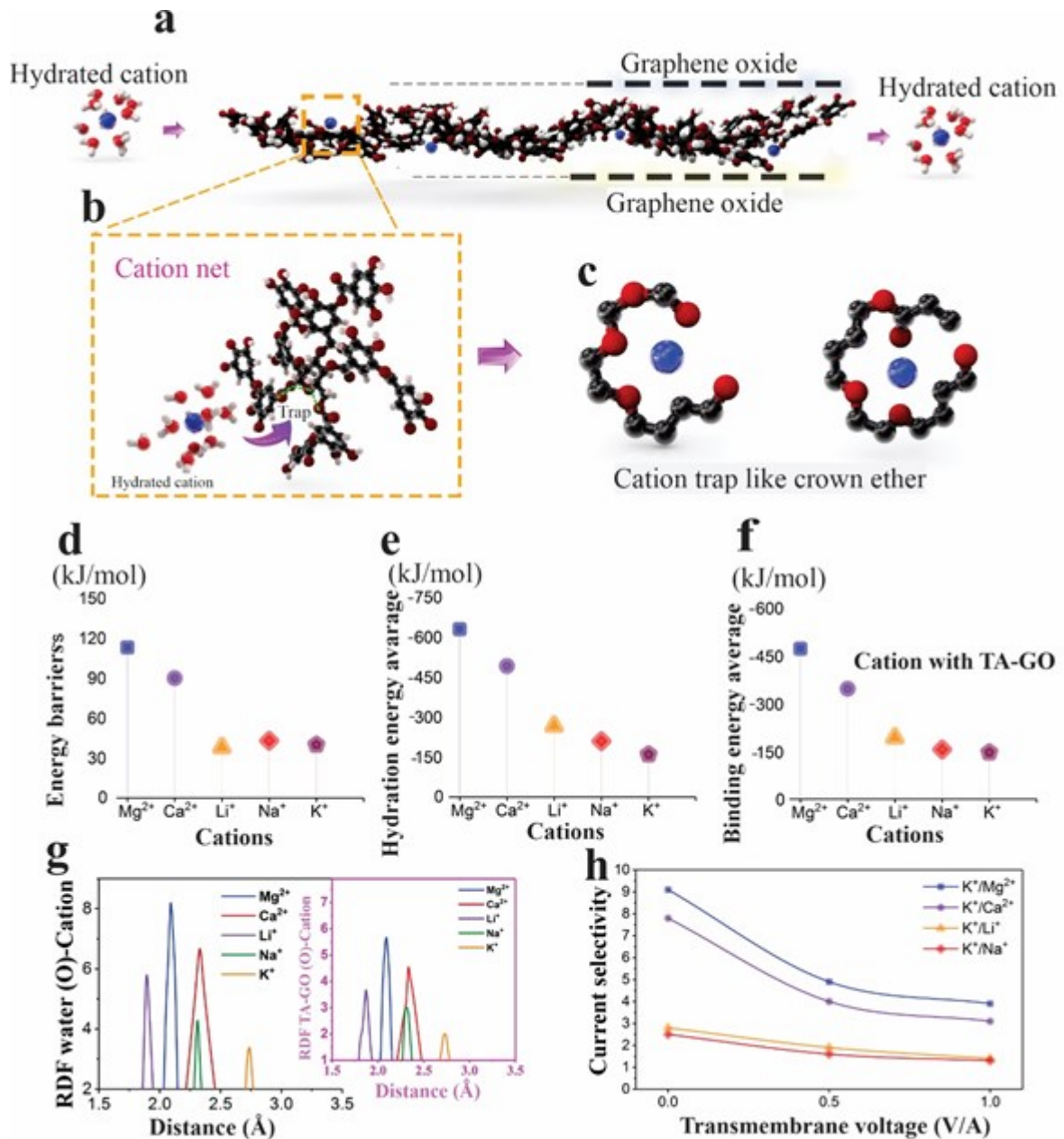


Figure 4. a) A snapshot of the TA-GO membrane showing that tannic acid acts like a net in the graphene oxide membrane, (b) An intrinsic trap in the structure of tannic acid, (c) Two trap models like crown ether that exist in tannic acid under extreme cavity, (d) The barrier energy of ions for penetrating, (e) The hydration energy of ions inside the TA-GO membrane, (f) The binding energy between ions and the TA-GO membrane, (g) RDF between ions and oxygen of water molecule and oxygen of TA-GO, and (h) The selectivity of K⁺ against other ions under the electric field. Grey, red, white and blue represents a carbon atom, an oxygen atom, hydrogen atom and cations, respectively.

To illustrate the role of the tannins, phenol groups, and hydroxyl groups considering their electrochemistry behaviour and the position of them in GO, we could say that this complex of oxygen atoms is similar to the defective crown ether but with the advantage of widespread distribution throughout the membrane.

By zooming on the strategic region of equilibrium adsorption distance for cations, we found two patterns of traps like defective crown ether that illustrated in **Figure 5a** and **5b**. As shown in Figure 5a, when ions are under interaction with the first model of cation traps in the TA-GO membrane, they experience huge binding energy which is the same meaning with trap energy. When cations, Mg^{2+} , Ca^{2+} , Li^+ , Na^+ and K^+ , are concentrated in the center of the trap, the cation trap energy is -695, -486, -273, -234, and -192 $KJ mol^{-1}$, respectively. For the second model of the cation trap, the trap energy for Mg^{2+} , Ca^{2+} , Li^+ , Na^+ and K^+ is -642, -546, -320, -253, and -211 $KJ mol^{-1}$, respectively. A review of the results of these two models shows that the trapping efficiency of the tannic acid molecule as a natural ion trapper is greater than other synthetic counterparts (See Table S3). With comparing Figure 4f with Figure 5a and b, the binding energy on two models of the trap with ions is significantly higher than natural interaction between oxygen functional groups in TA-GO membrane with ions, which confirms our hypothesis.

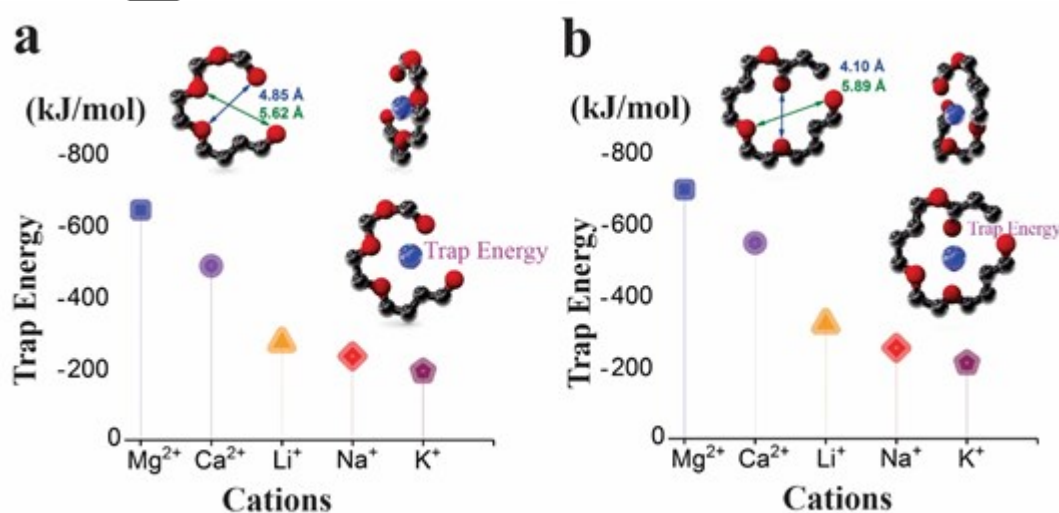


Figure 5. Shows two models of the cation trap in TA-GO created from tannins, phenol groups, and hydroxyl groups under confined space of graphene oxide layers, (a) the trap energy for ions when they are in the centre of the first model of cation trap, and (b) the trap energy for ions when they are in the centre of the second model of cation trap. Grey, red, white and blue represents a carbon atom, an oxygen atom, hydrogen atom and cations, respectively.

4. Conclusion

In this study, the effect of functionalising a free-standing GO-based membrane with a natural polyphenol (TA) on ion transportation inside the nanochannel was experimentally and theoretically investigated. The measurement of ionic currents through the TA-GO ED cell showed that it has the potential to contribute efficiently to the in-demand lithium extraction process. Testing different electrolytes of matching ionic concentration indicated that ionic conductance for Li^+ is less than other monovalent ions, which leads to the exclusion of Li^+ from other single-charged cations. Furthermore, the results obtained from the ion penetration test exhibited a much higher permeation flux for K^+ and Na^+ in comparison with Li^+ and other tested divalent ions. The obtained results showed that the Li^+ trapping capability of the membrane compared to K^+ and Na^+ is 1.49, and 1.18 respectively which results in lithium enrichment in the feed compartment. These values are higher than those of other membranes reported in the literature. As a new concept, the MD simulations revealed that the formation of natural nano nets consisting of continuous crown-shaped ether structures due to the introduction of tannic acid inside GO nanolayers leads to significant enhancement of the ion trapping process, and consequently membrane selectivity compared to similar GO-based membranes reported previously in the literature. Also, the results obtained from simulation showed that the effect of the tannic acid diffusion barrier on the permeation of monovalent and divalent cations varies between ions. Examination of the barrier, hydration and binding energies indicates that Li-ion experiences a higher resistance to entry to the nanochannel and disassembly from the TA-GO structure compared to the other monovalent cations studied, but that its resistance is lower than that for the divalent cations. The trapping energy of membrane is found to be -593, 487 and -403 KJ mol^{-1} for Li^+ , Na^+ and K^+ respectively.

Furthermore, the comparison between the trapping energy of the TA crown-like structure and other synthetic crown ether shows the great efficiency of TA-GO membrane to trap target ions. Based on the excellent agreement between experimental and simulation results, the authors believe that the use of this novel concept provides researchers with new methods for Li-ion separation and optimizes its industrial application.

5. Materials and methods

Chemicals and Materials: GO powder and all salts used in this study (potassium chloride (KCl), sodium chloride (NaCl), lithium chloride (LiCl), calcium chloride and magnesium chloride (MgCl_2)) were supplied by Sigma-Aldrich and used without change. Polydimethylsiloxane (PDMS) was provided by Sylgard 184, Dow Corning Australia. Milli-Q water with the resistivity of $11.6 \mu\text{S}/\text{cm}$ was used to produce the electrolyte solution in all tests.

Preparation of Tannic acid-functionalized GO membrane: A flat sheet of Polypropylene (PP) membrane was used as the substrate for the tannic acid-functionalized GO composite membrane. The substrate was wetted in ethanol for 24 h before vacuum filtration. Tannic acid (1 mg/ml) was dissolved in Bis-Tris buffer (100 mM buffer and pH 7.0). Then, GO powder (0.02 mg/ml) was added into the solution of tannic acid and Tris-buffer. The mixture was sonicated for 30 mins. After that, the GO with the tannic acid mixture was filtered through the PP membrane under vacuum filtration with a GO and TA loading of $0.137 \text{ mg}/\text{cm}^2$ and $6.6 \text{ mg}/\text{cm}^2$, respectively.

Characterization: X-ray diffraction (XRD) scans in the 2θ range of $5\text{-}50^\circ$ were taken utilizing the Empyrean PANalytical thin-film XRD with a Co $K\alpha$ ($\lambda=1.79 \text{ \AA}$) radiation source at a voltage of 40 kV and a scanning speed of $5.0^\circ \text{ min}^{-1}$ to measure the interlayer spacing of the tannic acid-functionalized GO composite membrane. The electrochemical tests were

conducted on a potentiostat (SP-300, BioLogic Science Instrument) where one of Ag/AgCl electrodes was used as the working electrode and another as both reference and counter electrodes. A field-emission electron microscope (FEI Nova SEM230) was used to characterize the tannic acid-functionalized GO composite membrane surface and cross-sectional morphology. To prepare free standing GO layers for SEM, a Whatman Anodisc alumina membrane with 47mm diameter and 0.2 μm pore size was used as the membrane substrate instead of the PP membrane. After drying, the GO layer was detached from the alumina membrane, and then peeled off TA-GO membrane used for measurement of the SEM cross-sectional image. This process was done to prevent GO layer damage during the preparation of the cross-sectional sample for SEM. Atomic force microscopy (AFM) using Bruker ScanAsyst-Air was accomplished to determine the surface roughness of the tannic acid-functionalized GO composite membrane, and the thickness of a single layer GO nanosheet. A Bruker FT-NIR/IR spectrometer was used to characterize the functional group of the tannic acid-functionalized GO composite membrane and the GO composite membrane without tannic acid. An Attension Theta Flex (Biolin Scientific) contact angle meter was used to measure the contact angles of the GO composite membrane and the tannic acid-functionalized GO composite membrane in order to determine the hydrophilicity of the membrane surface by the sessile drop method. The size of the water droplet was 3 μL . A TA Instruments Q5000 thermogravimetric analyser was used to measure the weight loss of TA/GO/PP, GO/PP and PP membranes as the temperature was ramped from room temperature to 700 $^{\circ}\text{C}$ at a rate of 10 $^{\circ}\text{C min}^{-1}$ under a nitrogen and oxygen atmosphere. The initial weight of the samples was approximately 5 mg for each measurement.

Electrodialysis (ED) in-house cell fabrication and cation conductivity test: Fabrication of the ED device required several steps as described below. In the first step, the flexible free-standing TA-GO membrane was cut into a rectangular shape 5 mm wide and 15 mm long.

Then two small cubes of cured PDMS with dimensions of 2 mm × 5 mm × 3 mm were bonded to the bottom of the plastic petri dish 10 mm apart using a micro-drop of a non-conductive epoxy. In the third step, the shaped membrane was mounted horizontally on the two PDMS stands to avoid any distortion in the membrane during the fabrication process. In the fourth step, the liquid blend of PDMS prepolymer and curing agent with a mass ratio of 1:20 was poured into the petri dish, covering the whole membrane to avoid any cracks on the GO nanosheet due to circumferential tension or pressures. After curing the PDMS in the oven at 50 °C for 45 minutes, two reservoirs each with approximate volume 1.0 mL were carved out of the PDMS elastomer to expose the two ends of GO-TA membrane to the ion-containing solution. Then the water was left in both reservoirs for 48 hours to ensure the full hydration of the nanochannels, which leads to the formation of 2D capillary channels.^[34] To ensure reaching steady-state conditions for conductivity measurements, the specified concentration of the corresponding salt was kept in both reservoirs for 24 hours prior to each test. Both Platinum and Ag/AgCl electrodes were considered for conductivity measurements in the early stages of the tests. It was found that the experiments with platinum electrodes suffer considerable error due to proton reduction around the electrodes (Figure S9). These results were in agreement with a previously reported study on electrochemical methods.^[31] Hence, the 2mm silver wire was coated with AgCl through an electrodeposition process to produce Ag/AgCl electrodes and inserted in the reservoirs to act as the source and drain. It should be noted that the electrodes should be in contact with both ends of the membrane to eliminate the effect of electrolyte resistance on conductivity results. Linear sweep voltammetry (LSV) tests were performed with the voltage ranging from -1.0 to 1.0 V with different salt concentrations varying in the range from 10⁻⁶ to 1 M to obtain the corresponding current-voltage (I-V) curves. Then the membrane conductance was calculated from the slope of each I-V curve and converted to a conductivity value by the formula $\lambda = G(l/hw)$ where G is

the measured conductance and l , h and w represent the length, height and width of the channel, respectively.^[40] Each measurement was repeated three times to calculate the average conductance and its standard error for the same setup.

Preparation of ED cell for permeation tests: In order to evaluate ionic flow rate through the TA-GO membrane, the ion permeation tests were conducted using the ED cell fabricated in-house as described in the previous section. Two etched reservoirs filled with Milli-Q water and salt solution were used as the feed and permeate compartments, and a 1.0 V electric field was applied for 30 minutes to drive ions to move through the membrane. The voltage was limited to 1.0 V to avoid the water splitting in the vicinity of the electrodes. A mixed solution of salts with 0.5M concentration of KCl, NaCl, LiCl, CaCl₂ and MgCl₂ was placed in the feed reservoir, with the other reservoir filled with Milli-Q water. The measurement of permeation rate was implemented by taking a sample from the permeate compartment and testing it employing inductively coupled plasma atomic emission spectrometer (ICP- AES, Agilent 4100). Therefore, the ratio of ions in the permeate would be the same as the ratio of ion permeation fluxes. Each measurement was repeated three times to ensure the reproducibility of the results and to obtain the standard error for the same setup.

Molecular dynamic (MD) simulation: Molecular dynamics simulation (MD) was used to investigate the behaviour of the cations in the TA-GO membrane. The simulations were carried out using Large-scale Atomic/Molecular Massively Parallel Simulator (LAMMPS) and Material Studio^[41] in the NVT ensemble at 298 K controlled via the Nose Hoover thermostat.^[42] The integration of motion equations was performed via the velocity Verlet method, with a time-step of 1 fs, and the periodic boundary conditions were imposed in all directions. The force field computations were conducted using the INTERFACE-PCFF force field, which describes the interactions in organic compounds, biomolecules and polymers. It should be noted that the INTERFACE force field operates as an extension of common PCFF,

COMPASS, CHARMM, AMBER, GROMACS, and OPLS-AA force fields. The non-bonded interactions, van der Waals, and the electrostatic interactions for the TA-GO nanochannel were represented by Lennard-Jones 6-9 and Coulombic functions, respectively.^[43] (see simulation model and more details in section 4 of supporting information)

Supporting Information

Supporting Information is available from the Wiley Online Library or from the author.

Acknowledgements

This work was supported by the Australian Research Council Centre Discovery Early Career Researcher Award (DECRA)DE180100688. The Funding is provided by the Australian Academy of Science, on behalf of the Department of Industry, Science, Energy and Resources. The Regional Collaborations Programme is supported by the Australian Government under the National Innovation and Science Agenda.

References

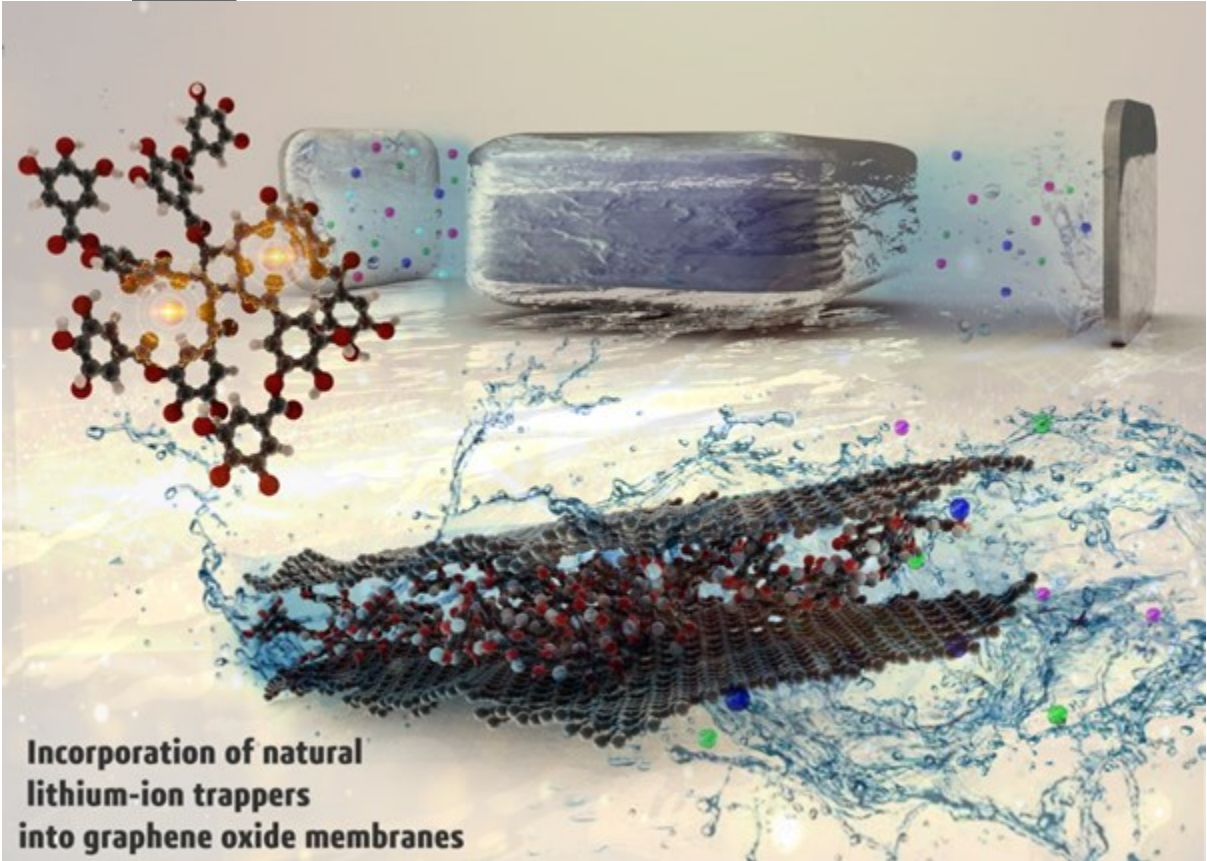
- [1] a) T. Tao, S. Lu, Y. Chen, *Advanced Materials Technologies* **2018**, *3*, 1700375; b) S. Choi, G. Wang, *Advanced Materials Technologies* **2018**, *3*, 1700376.
- [2] P. K. Choubey, K.-S. Chung, M.-s. Kim, J.-c. Lee, R. R. Srivastava, *Minerals Engineering* **2017**, *110*, 104.
- [3] a) A. Razmjou, M. Asadnia, E. Hosseini, A. Habibnejad Korayem, V. Chen, *Nature Communications* **2019**, *10*, 5793; b) A. Razmjou, G. Eshaghi, Y. Orooji, E. Hosseini, A. H. Korayem, F. Mohagheghian, Y. Boroumand, A. Noorbakhsh, M. Asadnia, V. Chen, *Water Research* **2019**, *159*, 313.
- [4] a) Q. Bi, Z. Zhang, C. Zhao, Z. Tao, *Water Science and Technology* **2014**, *70*, 1690; b) W. Li, C. Shi, A. Zhou, X. He, Y. Sun, J. Zhang, *Separation and Purification Technology* **2017**, *186*, 233; c) A. Somrani, A. H. Hamzaoui, M. Pontie, *Desalination* **2013**, *317*, 184; d) H.-Z. Zhang, Z.-L. Xu, H. Ding, Y.-J. Tang, *Desalination* **2017**, *420*, 158.
- [5] P. K. Choubey, M.-s. Kim, R. R. Srivastava, J.-c. Lee, J.-Y. Lee, *Minerals Engineering* **2016**, *89*, 119.
- [6] S. Gao, D. Wang, W. Fang, J. Jin, *Advanced Materials Technologies* **2020**, *5*, 1901069.
- [7] a) J. Abraham, K. S. Vasu, C. D. Williams, K. Gopinadhan, Y. Su, C. T. Cherian, J. Dix, E. Prestat, S. J. Haigh, I. V. Grigorieva, P. Carbone, A. K. Geim, R. R. Nair, *Nature Nanotechnology* **2017**, *12*, 546; b) W. Choi, Z. W. Ulissi, S. F. E. Shimizu, D. O. Bellisario, M. D. Ellison, M. S. Strano,

- Nature Communications* **2013**, *4*, 2397; c) P. Wang, M. Wang, F. Liu, S. Ding, X. Wang, G. Du, J. Liu, P. Apel, P. Kluth, C. Trautmann, Y. Wang, *Nature Communications* **2018**, *9*, 569.
- [8] a) M. Ali, I. Ahmed, P. Ramirez, S. Nasir, S. Mafe, C. M. Niemeyer, W. Ensinger, *Analytical Chemistry* **2018**, *90*, 6820; b) T. Gamble, K. Decker, T. S. Plett, M. Pevarnik, J.-F. Pietschmann, I. Vlasiouk, A. Aksimentiev, Z. S. Siwy, *The Journal of Physical Chemistry C* **2014**, *118*, 9809.
- [9] a) Y. Guo, Y. Ying, Y. Mao, X. Peng, B. Chen, *Angewandte Chemie International Edition* **2016**, *55*, 15120; b) C. E. Ren, K. B. Hatzell, M. Alhabeab, Z. Ling, K. A. Mahmoud, Y. Gogotsi, *The Journal of Physical Chemistry Letters* **2015**, *6*, 4026; c) Q. Wen, D. Yan, F. Liu, M. Wang, Y. Ling, P. Wang, P. Kluth, D. Schauries, C. Trautmann, P. Apel, W. Guo, G. Xiao, J. Liu, J. Xue, Y. Wang, *Advanced Functional Materials* **2016**, *26*, 5947.
- [10] Q. Pu, J. Yun, H. Temkin, S. Liu, *Nano Letters* **2004**, *4*, 1099.
- [11] a) M. Asadnia, M. Myers, N. D. Akhavan, K. O'Donnell, G. A. Umana-Membreno, U. Mishra, B. Nener, M. Baker, G. Parish, *Analytica chimica acta* **2016**, *943*, 1; b) T. M. Sanders, M. Myers, M. Asadnia, G. A. Umana-Membreno, M. Baker, N. Fowkes, G. Parish, B. Nener, *Sensors and Actuators B: Chemical* **2017**, *250*, 499.
- [12] W. Stillwell, in *An Introduction to Biological Membranes (Second Edition)* (Ed: W. Stillwell), Elsevier **2016**, p. 423.
- [13] M. Kazemabad, A. Verliefde, E. R. Cornelissen, A. D'Haese, *Journal of Membrane Science* **2020**, *595*, 117432.
- [14] a) R. Mohammad Zadeh Kakhki, G. Rounaghi, *Journal of Chemical & Engineering Data* **2011**, *56*, 3169; b) B. Swain, *Journal of Chemical Technology & Biotechnology* **2016**, *91*, 2549.
- [15] A. Gherrou, H. Kerdjoudj, R. Molinari, P. Seta, *Materials Science and Engineering: C* **2005**, *25*, 436.
- [16] a) T. Hayashita, R. A. Bartsch, *Analytical Chemistry* **1991**, *63*, 1847; b) Q. Zhao, R. A. Bartsch, *Journal of Applied Polymer Science* **1995**, *57*, 1465.
- [17] L. A. Limjoco, G. M. Nisola, R. E. C. Torrejos, J. W. Han, H. S. Song, K. J. Parohinog, S. Koo, S.-P. Lee, W.-J. Chung, *ACS Applied Materials & Interfaces* **2017**, *9*, 42862.
- [18] K. R. Bang, D. Bahamon, L. F. Vega, E. S. Cho, *Advanced Materials Interfaces* **2020**, *n/a*, 1901876.
- [19] Y. Kang, Y. Xia, H. Wang, X. Zhang, *Advanced Functional Materials* **2019**, *29*, 1902014.
- [20] Y. Zhao, W. Shi, B. Van der Bruggen, C. Gao, J. Shen, *Advanced Materials Interfaces* **2018**, *5*, 1870025.
- [21] F. Fei, L. Cseri, G. Szekely, C. F. Blanford, *ACS Applied Materials & Interfaces* **2018**, *10*, 16140.
- [22] a) Y. Yang, Y. Li, Q. Li, Y. Wang, C. H. Tan, R. Wang, *Journal of Membrane Science* **2019**, *588*, 117203; b) H. M. Hegab, A. ElMekawy, T. G. Barclay, A. Michelmore, L. Zou, C. P. Saint, M. Ginic-Markovic, *ACS Applied Materials & Interfaces* **2016**, *8*, 17519.
- [23] a) A. Alabi, L. Cseri, A. Al Hajaj, G. Szekely, P. Budd, L. Zou, *Journal of Membrane Science* **2020**, *594*, 117457; b) A. Alammari, S.-H. Park, C. J. Williams, B. Derby, G. Szekely, *Journal of Membrane Science* **2020**, *603*, 118007.
- [24] L. Pan, H. Wang, C. Wu, C. Liao, L. Li, *ACS Applied Materials & Interfaces* **2015**, *7*, 16003.
- [25] a) M.-Y. Lim, Y.-S. Choi, J. Kim, K. Kim, H. Shin, J.-J. Kim, D. M. Shin, J.-C. Lee, *Journal of Membrane Science* **2017**, *521*, 1; b) K. H. Thebo, X. Qian, Q. Zhang, L. Chen, H.-M. Cheng, W. Ren, *Nature Communications* **2018**, *9*, 1486.
- [26] M.-Y. Lim, H. Shin, D. M. Shin, S.-S. Lee, J.-C. Lee, *Polymer* **2016**, *84*, 89.
- [27] O. M. Slobodian, P. M. Lytvyn, A. S. Nikolenko, V. M. Naseka, O. Y. Khyzhun, A. V. Vasin, S. V. Sevostianov, A. N. Nazarov, *Nanoscale Research Letters* **2018**, *13*, 139.
- [28] a) H. J. Kim, Y.-S. Choi, M.-Y. Lim, K. H. Jung, D.-G. Kim, J.-J. Kim, H. Kang, J.-C. Lee, *Journal of Membrane Science* **2016**, *514*, 25; b) R. Liu, H. Ge, X. Wang, J. Luo, Z. Li, X. Liu, *New Journal of Chemistry* **2016**, *40*, 6332.

- [29] a) C.-Y. Tang, P. Yu, L.-S. Tang, Q.-Y. Wang, R.-Y. Bao, Z.-Y. Liu, M.-B. Yang, W. Yang, *Ecotoxicology and Environmental Safety* **2018**, *165*, 299; b) X. Zhao, M. Gnanaseelan, D. Jehnichen, F. Simon, J. Pionteck, *Journal of Materials Science* **2019**, *54*, 10809.
- [30] A. R. Chaharmahali, *Sydney: The University of New South Wales* **2012**.
- [31] A. J. Bard, L. R. Faulkner, J. Leddy, C. G. Zoski, *Electrochemical methods: fundamentals and applications*, Wiley New York, **1980**.
- [32] a) A. R. Koltonow, J. Huang, *Science* **2016**, *351*, 1395; b) R. B. Schoch, J. Han, P. Renaud, *Reviews of Modern Physics* **2008**, *80*, 839; c) D. Stein, M. Kruithof, C. Dekker, *Physical Review Letters* **2004**, *93*, 035901.
- [33] a) L. J. Cheng, L. J. Guo, *Nano Letters* **2007**, *7*, 3165; b) W. Guan, R. Fan, M. A. Reed, *Nature Communications* **2011**, *2*, 506.
- [34] R. R. Nair, H. A. Wu, P. N. Jayaram, I. V. Grigorieva, A. K. Geim, *Science* **2012**, *335*, 442.
- [35] L. Chen, G. Shi, J. Shen, B. Peng, B. Zhang, Y. Wang, F. Bian, J. Wang, D. Li, Z. Qian, G. Xu, G. Liu, J. Zeng, L. Zhang, Y. Yang, G. Zhou, M. Wu, W. Jin, J. Li, H. Fang, *Nature* **2017**, *550*, 380.
- [36] B. Tansel, *Separation and purification technology* **2012**, *86*, 119.
- [37] a) A. Razmjou, M. R. Barati, G. P. Simon, K. Suzuki, H. Wang, *Environmental Science & Technology* **2013**, *47*, 6297; b) S. Sahu, M. Di Ventra, M. Zwolak, *Nano Letters* **2017**, *17*, 4719.
- [38] J. N. Israelachvili, *Intermolecular and surface forces*, Academic press, **2015**.
- [39] A. Razmjou, *Advanced Materials Interfaces* **2019**, *6*, 1801427.
- [40] K. Raidongia, J. Huang, *Journal of the American Chemical Society* **2012**, *134*, 16528.
- [41] E. Hosseini, M. Zakertabrizi, A. Habibnejad Korayem, R. Shahsavari, *ACS applied materials & interfaces* **2019**, *11*, 8635.
- [42] a) E. Hosseini, M. Zakertabrizi, A. H. Korayem, S. Chen, S. K. Mohsenabadi, *Construction and Building Materials* **2019**, *224*, 266; b) W. G. Hoover, *Physical review A* **1985**, *31*, 1695; c) S. Nosé, *Molecular physics* **1984**, *52*, 255.
- [43] a) H. Heinz, T.-J. Lin, R. Kishore Mishra, F. S. Emami, *Langmuir* **2013**, *29*, 1754; b) R. K. Mishra, L. Fernández-Carrasco, R. J. Flatt, H. Heinz, *Dalton Transactions* **2014**, *43*, 10602.

Author Manuscript

ript



Authc

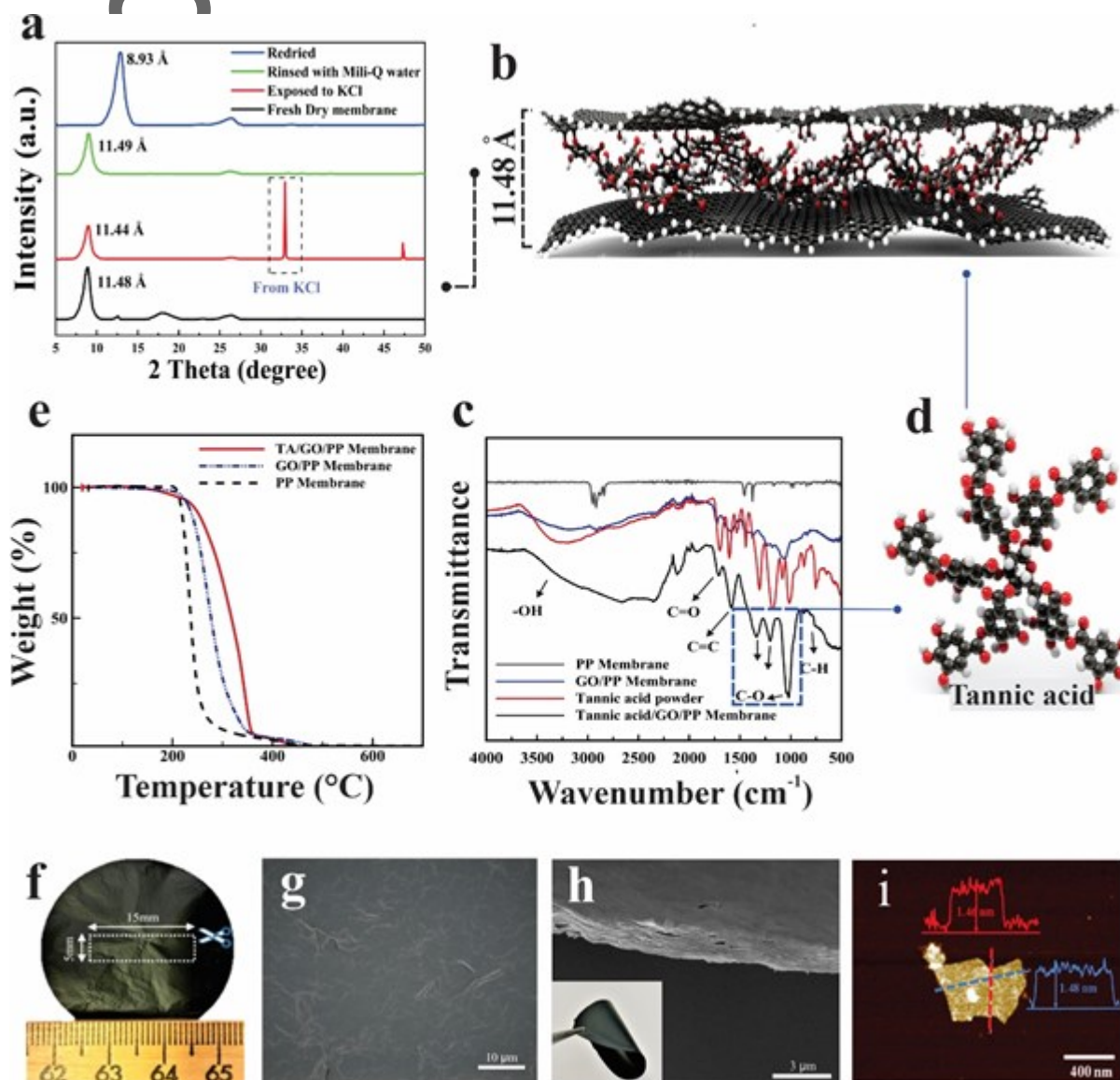


Figure 6. Characterisation of fabricated TA-GO membrane. (a) XRD patterns of a fresh dry TA-GO membrane (black line), hydrated TA-GO membrane exposed to 1M KCl (red line), rinsing the exposed TA-GO membrane with Milli-Q water (green line) and redried TA-GO membrane (blue line), (b) Molecule view of TA inside GO nanochannel size. , (c) FTIR spectra of a TA-GO/PP membrane (black line), a GO/PP membrane (blue line), and PP membrane (grey line), (d) Schematic illustration of TA structure and functional groups. , (e) Thermogravimetric analysis (TGA) of TA-GO/PP membrane (red line), a GO/PP membrane (dashed blue line), and PP membrane (dashed black line), (f) Digital photograph of the rectangular-shaped strip with specific dimensions on TA-GO film, (g) SEM image of TA-GO membrane from the top view, (h) Cross-sectional SEM image of flexible TA-GO membrane, (i) AFM image of a single layer TA-GO sheet and the corresponding height profile in two different directions.

Author Manuscript

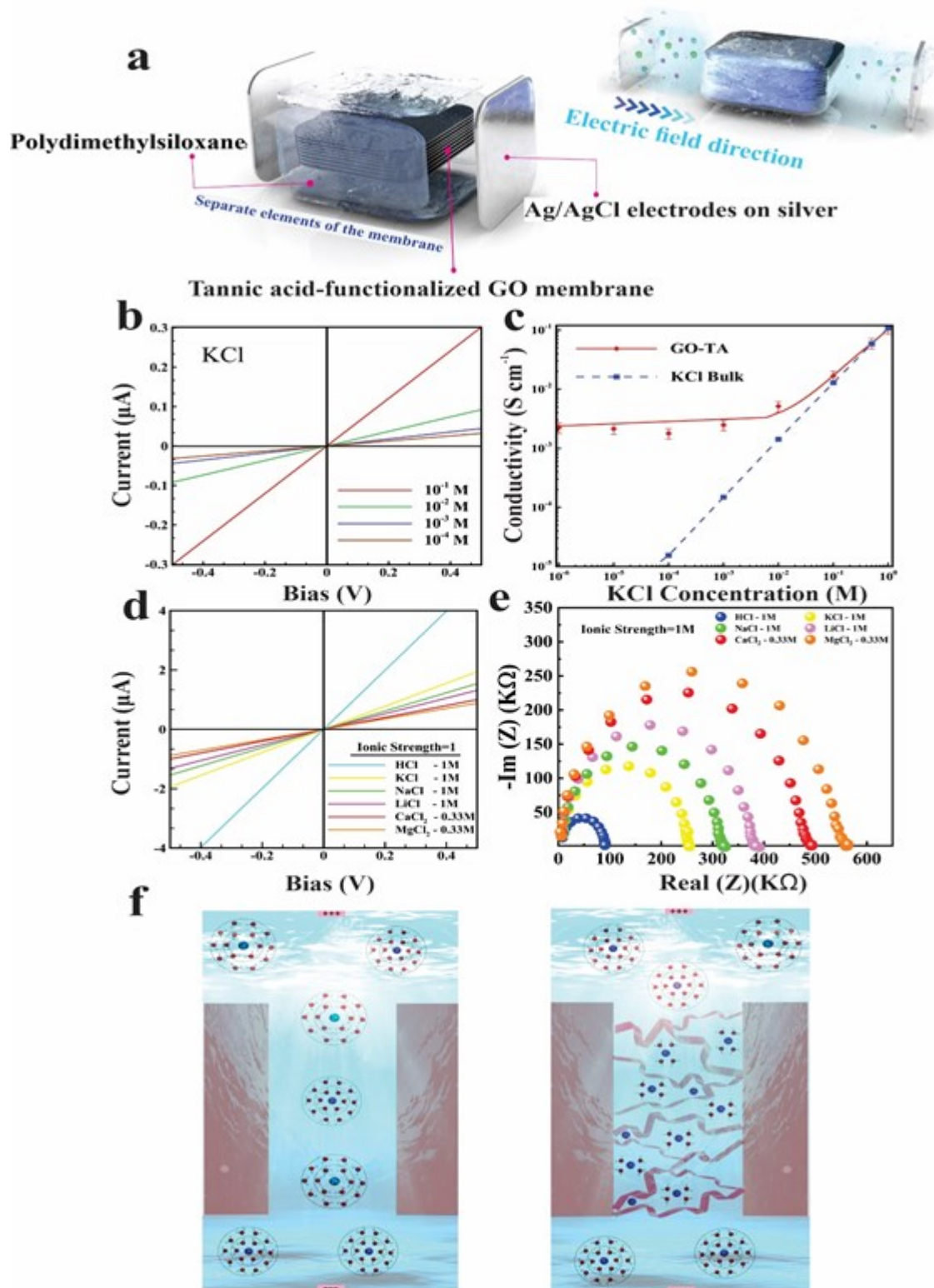


Figure 7. Ion transportation through TA-functionalized GO nanochannel. (a) Schematic view of separate elements of the membrane and snapshot of membrane design for ionic flow., (b) Representative I-V curves obtained at different KCl concentrations from 10^{-4} to 10^{-1} M, (c) Ionic conductivity as a function of the KCl concentration from 10^{-6} to 1 M, (d) A comparison between I-V curves of TA-GO membrane recorded for different electrolyte solutions at the same ionic strength, (e) Nyquist plots of TA-GO membrane recorded for different electrolyte solutions at the same ionic strength, (f) Ion transportation mechanism through GO

nanochannels with/without the presence of TA (spheres: light blue= Cl^- , dark blue = cation ions that are surrounded by H_2O molecules. “+” sign is Cathode while “-” sign is Anode).

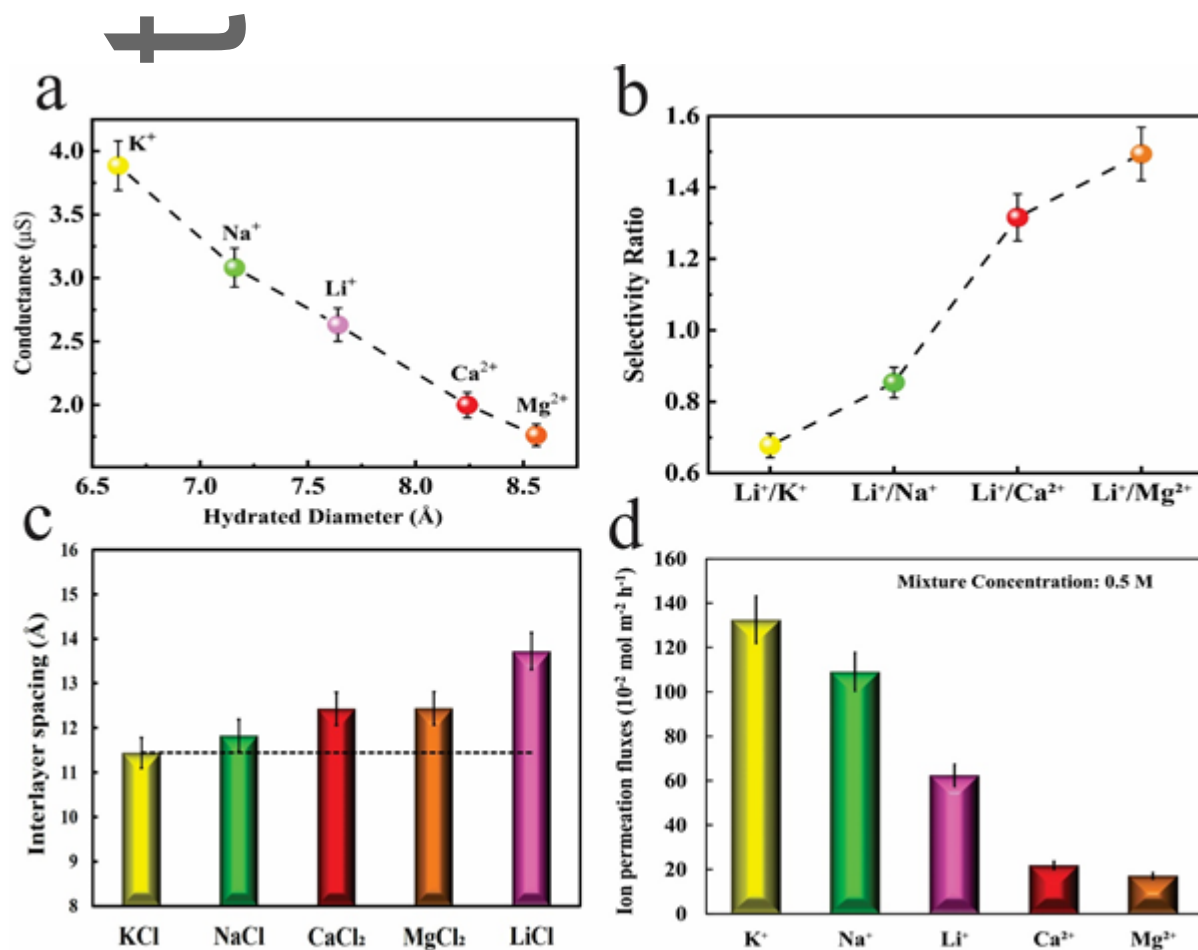


Figure 8. Effect of hydrated radii and chemical properties of cations on the transportation behaviour through the TA-GO nanochannel, (a) Variation of membrane's conductance with hydrated diameter of cations, (b) Comparison between the measured selectivity ratio of Li^+ to other cations, (c) Variation of nanochannel d-spacing due to exposing the TA-GO membrane to 5 different salt solutions, (d) Evaluation of ion permeation fluxes of 0.5 M mixed salts solution through TA-GO membrane at 1.0 V applied electric field using an ICP test.

Auth

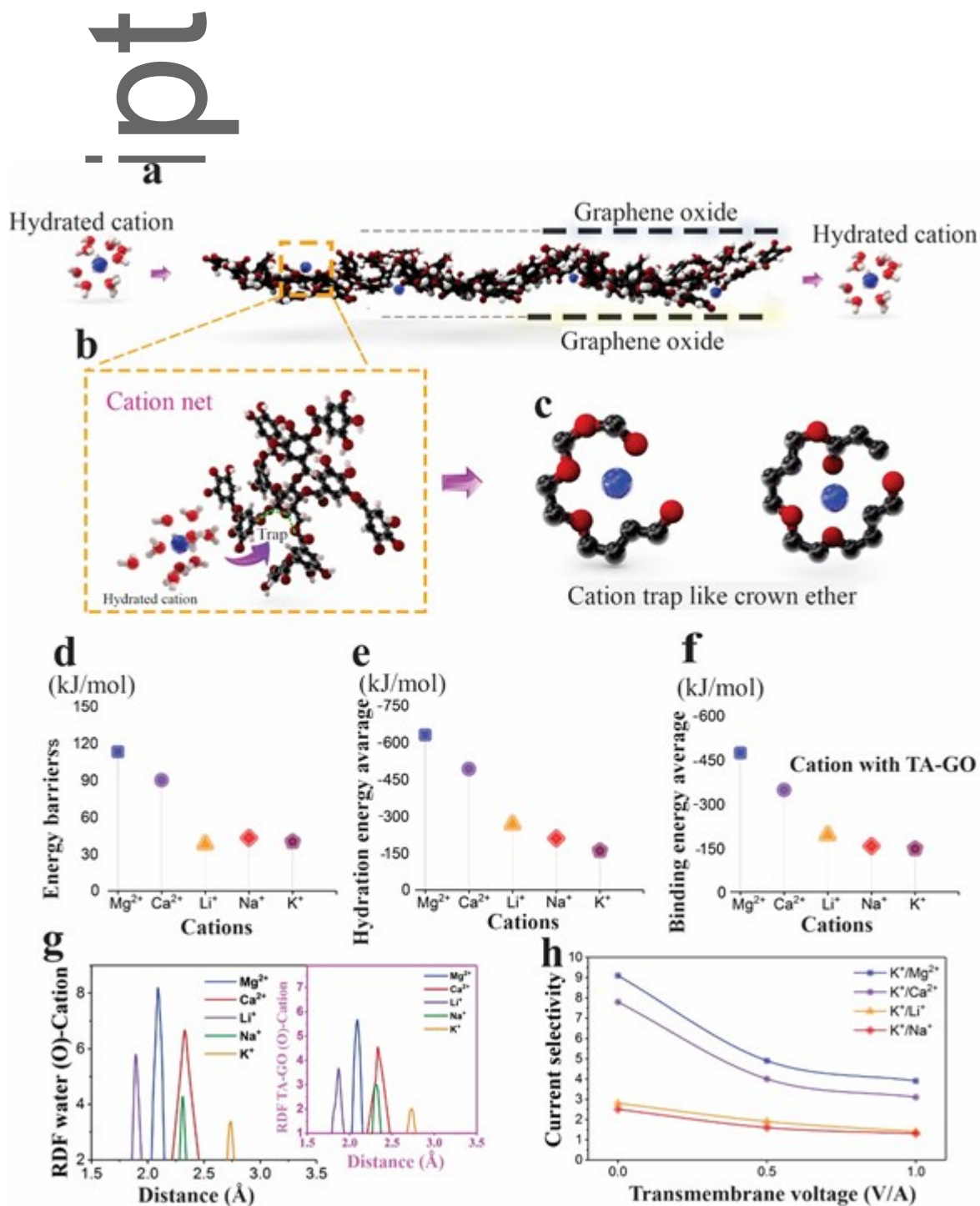


Figure 9. a) A snapshot of the TA-GO membrane showing that tannic acid acts like a net in the graphene oxide membrane, (b) An intrinsic trap in the structure of tannic acid, (c) Two trap models like crown ether that exist in tannic acid under extreme cavity, (d) The barrier energy of ions for penetrating, (e) The hydration energy of ions inside the TA-GO membrane, (f) The binding energy between ions and the TA-GO membrane, (g) RDF between ions and oxygen of water molecule and oxygen of TA-GO, and (h) The selectivity of K⁺ against other ions under the electric field. Grey, red, white and blue represents a carbon

atom, an oxygen atom, hydrogen atom and cations, respectively.

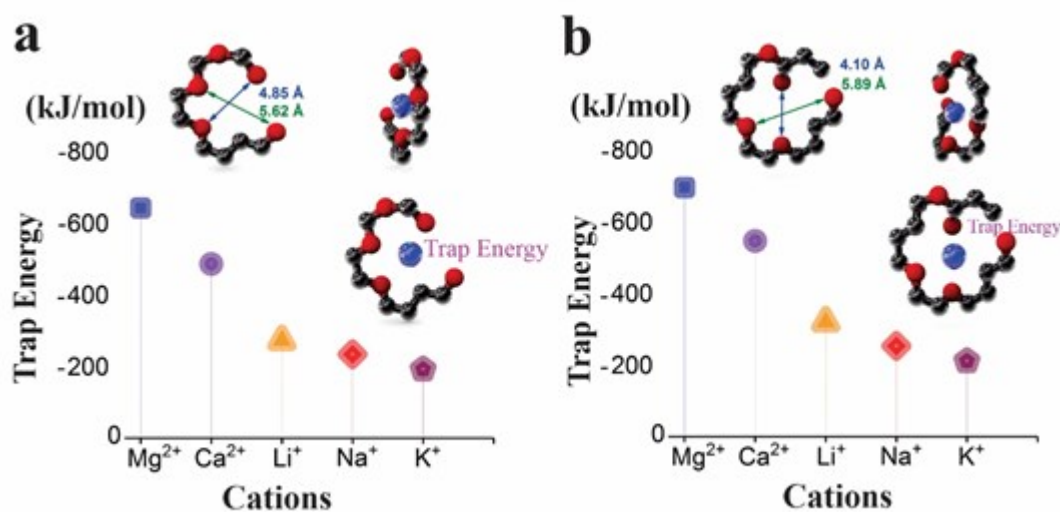


Figure 10. Shows two models of the cation trap in TA-GO created from tannins, phenol groups, and hydroxyl groups under confined space of graphene oxide layers, (a) the trap energy for ions when they are in the centre of the first model of cation trap, and (b) the trap energy for ions when they are in the centre of the second model of cation trap. Grey, red, white and blue represents a carbon atom, an oxygen atom, hydrogen atom and cations, respectively.

Intercalation of tannic acid as a natural crown ether-like structured ion trapper inside graphene oxide nanochannel results in the formation of natural cation nano net. The results from this study show the satisfactory performance of this nano net in exclusion of Lithium ions from other monovalent cations. This proof-of-concept introduces a novel design for 2D Li ion selective membranes.

